Glycopeptide from mountain-cultivated ginseng attenuates oxidant-induced cardiomyocyte and skeletal myoblast injury

Dongyue Zhou[1], Xuan Hu[1], Tongchuan Wu[1], Xue Li[1], Di Yang[1], Xingyu Tao[1], Yunhua Fu[1], Fei Zheng[1], Yulin Dai[1], Hao Yue[1], and YouJin Jeon[2]

[1]Changchun University of Chinese Medicine
[2]Jeju National University

February 2, 2023

Abstract

Background and purpose In Asian traditional medicine, ginseng has been referred to as the "King of Herbs" because to its extensive therapeutic and pharmacologic characteristics, particularly in the treatment of type 2 diabetes mellitus and illnesses connected to diabetes. Experimental approach The 80% ethanol extracts of cultivated, red, and mountain-cultivated ginseng were liquid partitioned with hexane, chloroform, ethyl acetate, and n-butanol, respectively. The residues produced were processed with enzyme-assisted extraction by different enzymes. Cardiomyocytes, skeletal myoblasts, wild-type AB line zebrafish and Tg (kdrl:EGFP) zebrafish were used to screen and verify the protective effect of extracts. Key results APMCG-1 is precipitated by alkaline protease-assisted extract from mountain-cultivated ginseng with 30% ethanol, which has a strong scavenging effect on hydroxyl radicals. In palmitic acid-induced H9c2 cells, APMCG-1 greatly enhanced cell viability while reducing reactive oxygen species generation and lactate dehydrogenase levels. Additionally, it reduced endoplasmic reticulum and mitochondrial dysfunction by increasing the Ca2+ level and membrane potential of mitochondria in H9c2(2-1) cells. In C2C12 cells that had been exposed to palmitic acid, APMCG-1 boosted glucose uptake while lowering creatine kinase levels. More significantly, 5 days after fertilization Tg (kdrl:EGFP) zebrafish and 1-month-old wild-type zebrafish with type 2 diabetic symptoms both had lower blood sugar and lipid levels attributed to APMCG-1. Further, APMCG-1 was identified as a glycopeptide containing O-linked glycopeptide bonds. Conclusions and implications As a PI3K/AKT activator, APMCG-1 protects the dysfunction of oxidant induced cardiomyocytes and skeletal myoblasts in type 2 diabetes, and is a potential therapeutic drug for diabetes.

Orcid ID:2023-BJP-0094-RP

Glycopeptide from mountain-cultivated ginseng attenuates oxidant-induced cardiomyocyte and skeletal myoblast injury

Authors:

Dongyue Zhou [a], Xuan Hu [a], Tongchuan Wu [a], Xue Li [a], Di Yang[a], Xingyu Tao [a], Yunhua Fu[a], Fei Zheng [a], Yulin Dai[a, *], Hao Yue [a, *], YouJin Jeon[b]

Affiliations: [a] Jilin Ginseng Academy, Changchun University of Chinese Medicine, Changchun 130117, China

[b] Department of Marine Life Science, Jeju National University, Jeju 63243, Republic of Korea

*Corresponding authors. Tel.: +86-431-8676-3986 fax: +86-431-8676-3986.

E-mail addresses: yuehao@ccucm.edu.cn (Hao Yue), daiyl@ccucm.edu.cn (Yulin Dai).

Data availability statement

The data that support the findings of this study are available from the corresponding author upon reasonable request. Some data may not be made available because of privacy or ethical restrictions.

Funding statement

This study was supported by the National Natural Science Foundation of China (No. 82204719), the Department of Science and Technology of Jilin Province (No. 20220204051YY, 20220508081RC, 20220401126YY).

Author contribution statement

Conceptualization: Hao Yue, Yulin Dai

Investigation: Fei Zheng, YouJin Jeon

Methodology: Dongyue Zhou, Xingyu Tao

Formal analysis: Xuan Hu, Di Yang

Writing - original draft: Dongyue Zhou, Yulin Dai

Writing - review and editing: Xue Li and Yunhua Fu, Tongchuan Wu

Conflict of interest disclosure

None of the authors declare conflict of interest.

Ethics approval statement

All the animal experiments were in line with the Animal Care & Welfare Committee of Changchun University of Chinese Medicine (Approval No.: 2022647).

Running title: Protective effects of glycopeptide in an experimental model of type 2 diabetes in zebrafish.

Major area: Pharmacology Biochemistry

Cross-cutting area: Pharmaceutical chemistry Pharmacoanalysis

Additional areas: Type 2 diabetes

What is already known

(1) Over twenty years growth mountain-cultivated ginseng as valuable plant contains active ingredients such as glycopeptide.

(2) Zebrafish is a well-known model of drug development for qualitative efficacy screening.

What this study adds

(1) The glycopeptide from mountain-cultivated ginseng is a potential treatment for glucose and lipid metabolism disorders, such as type 2 diabetes.

(2) Alkaline protease-assisted extract of mountain-cultivated ginseng could activate the PI3K/AKT signaling pathway of cardiomyocytes and skeleton myoblasts by zebrafish experiments.

Clinical significance

(1) In type 2 diabetes mellitus, APMCG-1, a PI3K/AKT activator, protects against oxidant-induced dysfunctions in skeletal myoblasts and cardiomyocytes.

(2) This finding provides fresh light on the potential of glycopeptides as a treatment for muscle-related conditions.

Background and purpose

In Asian traditional medicine, ginseng has been referred to as the "King of Herbs" because to its extensive therapeutic and pharmacologic characteristics, particularly in the treatment of type 2 diabetes mellitus and illnesses connected to diabetes.

Experimental approach

The 80% ethanol extracts of cultivated, red, and mountain-cultivated ginseng were liquid partitioned with hexane, chloroform, ethyl acetate, and n-butanol, respectively. The residues produced were processed with enzyme-assisted extraction by different enzymes. Cardiomyocytes, skeletal myoblasts, wild-type AB line zebrafish and Tg (kdrl:EGFP) zebrafish were used to screen and verify the protective effect of extracts.

Key results

APMCG-1 is precipitated by alkaline protease-assisted extract from mountain-cultivated ginseng with 30% ethanol, which has a strong scavenging effect on hydroxyl radicals. In palmitic acid-induced H9c2 cells, APMCG-1 greatly enhanced cell viability while reducing reactive oxygen species generation and lactate dehydrogenase levels. Additionally, it reduced endoplasmic reticulum and mitochondrial dysfunction by increasing the Ca^{2+} level and membrane potential of mitochondria in H9c2(2-1) cells. In C2C12 cells that had been exposed to palmitic acid, APMCG-1 boosted glucose uptake while lowering creatine kinase levels. More significantly, 5 days after fertilization Tg (kdrl:EGFP) zebrafish and 1-month-old wild-type zebrafish with type 2 diabetic symptoms both had lower blood sugar and lipid levels attributed to APMCG-1. Further, APMCG-1 was identified as a glycopeptide containing O-linked glycopeptide bonds.

Conclusions and implications

As a PI3K/AKT activator, APMCG-1 protects the dysfunction of oxidant induced cardiomyocytes and skeletal myoblasts in type 2 diabetes, and is a potential therapeutic drug for diabetes.

Keywords Mountain-cultivated ginseng Glycopeptides Type 2 diabetes mellitus Zebrafish Cardiomyocytes Skeletal myoblasts

Graphical Abstract

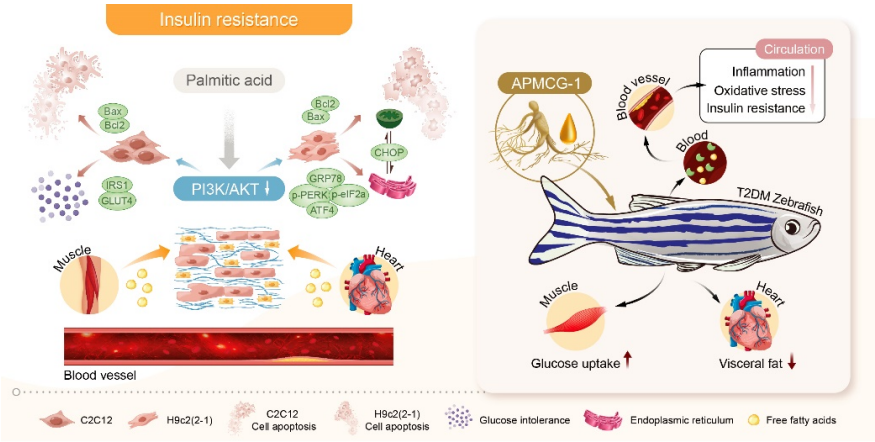

Abbreviations

AKT: protein kinase B

APMCG: alkaline protease-assisted extract from mountain-cultivated ginseng

ATF4: activating transcription factor 4

Bax: Bcl2-Associated x

Bcl2: B-cell lymphoma-2

CAE: crude aqueous extract

CAT: catalase

CHOP: C/EBP-homologous protein

CG: cultivated ginseng

CK: creatine kinase

CK-MB: creatine kinase isoenzyme

cTnI: ardiac troponin I

Cleaved-Caspase3: Cleaved-Cysteinyl aspartate specific proteinase 3

Cleaved-Caspase9: Cleaved-Cysteinyl aspartate specific proteinase 9

DAPI: 2-(4-Amidinophenyl)-6-indolecarbamidine dihydrochloride

DCFH-DA: dichloro-dihydro-fluorescein diacetate

DMEM: Dulbecco's Modified Eagle Medium

DPPH: 2, 2-diphenyl-1-picrylhydrazyl

ER: endoplasmic reticulum

eIF2α: eukaryotic translation initiation factor 2a

FBG: fasting blood glucose

FFA: free fatty acid

GSH-PX: glutathione peroxidase

FITC: fluorescein isothiocyanate

FT-IR: Fourier transform infrared spectroscopy

GLUT4: glucose transporter type 4

GPC: permeation chromatography

GRP78: glucose-regulated protein 78

HE: hematoxylin-eosin

Hoechst33342: 2'-[4-ethoxyphenyl]-5-[4-methyl-1-piperazinyl]-2,5'-bi-1H-benzimidazole trihydrochloride trihydrate

HPLC: high-performance liquid chromatography

IHC: immunohistochemistry

IL-6: interleukin-6

INS: insulin

IRS1: insulin receptor substrate 1

LDH: lactate dehydrogenase

MCG: mountain cultivated ginseng

MDA: malondialdehyde

MG: muscle glycogen

MTT: 3-(4, 5-dimethythiazol-2-yl)-2, 5-diphenyl tetrazolium bromide

mTOR: mammalian target of rapamycin

O^{2-}: superoxide anion radical

OH^{-}: hydroxyl free radical

PA: palmitic acid

p-AKT: phosphorylation- protein kinase B

PBS: phosphate-buffered saline

p-eIF2α: phosphorylation-eukaryotic translation initiation factor 2a

PERK: protein kinase R-like endoplasmic reticulum kinase

p-PERK: phosphorylation-protein kinase R-like endoplasmic reticulum kinase

PI: propidium iodide

PI3K: phosphatidylinositol-3 kinase

PMP: 1-phenyl-3-methyl-5-pyrazolone

RG: red ginseng

ROS: reactive oxygen species

SOD: superoxide dismutase

T-CHO: total-cholesterol

TCM: traditional Chinese medicine

TG: triglyceride

TNF-a: tumor necrosis factor-a

TUNEL: TdT-mediated dUTP Nick-End Labeling

T2DM: type 2 diabetes mellitus

UV: ultraviolet

Introduction

Diabetes mellitus raises the risk of heart failure and skeletal muscle dysfunction, which is responsible for reduced exercise capacity commonly observed in heart failure (Cui et al., 2022). In cardiomyocytes, excess lipid droplets occurring in diabetes cause mitochondrial dysfunction in diabetic cardiomyopathy (Abel, 2018). Lipid overload in the endoplasmic reticulum (ER) led to ER stress and increased levels of reactive oxygen species (ROS), causing mitochondrial dysfunction and further promoting the progression of heart failure and muscle wasting (Frontera & Ochala, 2015; Ohsaki et al., 2017). Fatty acids maintain contractile function in cardiac and skeletal muscles. The uptake and β-oxidation of fatty acids are coordinately regulated to meet a sufficient supply for mitochondrial β-oxidation (Zhang et al., 2010). Mitochondrial dysfunction and inhibition of myoblast differentiation are mainly observed in diabetes (Jung & Mun, 2019), and they cause the failure of the skeletal myoblast to maintain normal function resulting in a weak exercise ability (Phielix & Mensink, 2008). The impaired function of the skeletal myoblast affects glucose metabolism, leading to diabetic myopathy (Sinacore & Gulve, 1993). Clinical and experimental evidence supports that activation of phosphatidylinositol-3 kinase (PI3K)/protein kinase B (AKT) /mammalian target of rapamycin (mTOR) (Xu et al., 2016) signaling pathway is a strategy for the treatment of skeletal muscle atrophy in individuals

with diabetes (Jiao et al., 2022). Thus, the functional changes of cardiomyocytes and skeletal myoblasts under type 2 diabetes mellitus (T2DM) conditions should be investigated.

More than 1500 traditional Chinese medicine (TCM) manufacturers yield up to 35 million tons of herbal solid wastes annually, and most of these waters are managed through landfills and incineration rather than considered as recyclable biomass (Tao et al., 2021). For ginseng extraction, water-insoluble ginsenosides are generally extracted by ethanol, and water-soluble ginsenosides polysaccharides/proteins are extracted by water (Sun et al., 2022). The extraction method applied by of TCM manufacturers uses either water or ethanol, resulting in a considerable amount of ethanol (or water)-insoluble active ingredients in herbal residues. Especially for the expensive mountain cultivated ginseng (MCG), functional substances make ginseng residues an attractive material in the field of active compounds. Recently, in China, the evident functional effect of *Panax ginseng* in attenuating the inflammatory response for the alleviation of COVID-19 has been reported, and it elicited great confidence and interest in the world (Yi, 2022). However, the mechanism of how MCG attenuates the cardiomyocyte and skeletal myoblast dysfunction is still unknown. Herein, three types of ginsengs were selected for screening and discovery of their protective effect on the heart and skeletal muscles under diabetic conditions. A total of 53 water or ethanol extracts were obtained from the ginsengs, and the sample with strongest properties was selected and for further characterized by analytical technologies.

Methods

Chemicals

Red ginseng (RG), cultivated ginseng (CG), and MCG were purchased from Fusong County, Jilin Province, China. Glycosylase, cellulase, a-amylase, β-glucanase, viscozyme®L, papain, compound protease, alkaline protease, neutral protease, chymotrypsin, catalase, trypsin, pepsin and dichloro-dihydro-fluorescein diacetate (DCFH-DA) were purchased from Shanghai Yuanye Bio-Technology Co., LTD. (Shanghai, China). 2, 2-diphenyl-1-picrylhydrazyl (DPPH), superoxide anion radical (O^{2-}), hydroxyl free radical (OH^{-}), creatine kinase (CK), lactate dehydrogenase (LDH), glucose, triglyceride (TG), total-cholesterol (T-CHO), superoxide dismutase (SOD), glutathione peroxidase (GSH-PX), catalase (CAT), malondialdehyde (MDA), tumor necrosis factor-a (TNF-a), interleukin-6 (IL-6), creatine kinase isoenzyme (CK-MB), cardiac troponin I (cTnI), insulin (INS), free fatty acid (FFA) and muscle glycogen (MG) kits were purchased from Nanjing Jiancheng Technology Co., LTD. (Nanjing, China). 3-(4, 5-dimethythiazol-2-yl)-2, 5-diphenyl tetrazolium bromide (MTT), fluo-8AM probe, 2'-[4-ethoxyphenyl]-5-[4-methyl-1-piperazinyl]-2,5'-bi-1H-benzimidazole trihydrochloride trihydrate (Hoechst 33342), propidium iodide (PI) and Rhodamine 123 probe were purchased from Beijing Soleibo Technology Co., LTD. (Beijing, China). AnnexinV-fluorescein isothiocyanate (FITC)/PI probe was purchased from Becton Dickinson (New Jersey, USA). Palmitic acid (PA) was purchased from Sigma (Schnelldorf, Germany). LY294002 was purchased from Med Chem Express (New Jersey, USA). PI3K, AKT, phosphorylation- protein kinase B (p-AKT), insulin receptor substrate 1 (IRS1), glucose transporter type 4 (GLUT4), Bcl2-Associated x (Bax), B-cell lymphoma-2 (Bcl2), Cleaved-Cysteinyl aspartate specific proteinase 3 (Cleaved-Caspase3), Cleaved-Cysteinyl aspartate specific proteinase 9(Cleaved-Caspase9), glucose-regulated protein 78 (GRP78), protein kinase R-like endoplasmic reticulum kinase (PERK), phosphorylation-protein kinase R-like endoplasmic reticulum kinase (p-PERK), eukaryotic translation initiation factor 2a (eIF2α), phosphorylation-eukaryotic translation initiation factor 2a (p-eIF2α), activating transcription factor 4 (ATF4) and C/EBP-homologous protein (CHOP) were purchased from Jiangsu Qinke Biological Research Center Co., LTD. (Jiangsu, China). TdT-mediated dUTP Nick-End Labeling (TUNEL) was purchased from Roche (Basel, Switzerland). 2-(4-Amidinophenyl)-6-indolecarbamidine dihydrochloride (DAPI) was purchased from Wuhan Borf Biotechnology Co., LTD. (Wuhan, China).

Extraction methods

A total of 200 g of RG, CG, and MCG were ground to powders. The ginsengs were degreased by petroleum ether for 12 h at room temperature. A concentration of 80% ethanol was used for the extracted ginsengs with a shaking speed of 180 rpm at 50 °C for 48 h. Subsequently, the extracts were liquid partitioned with

hexane, chloroform, ethyl acetate, and$n$ -butanol, respectively.

Enzyme-assisted extraction was followed by the previous protocol with slight modification (Lee et al., 2021): the ethanol extract residue was collected and decolorized by pure ethanol. The residue was further extracted by different enzymes (glycosylase, cellulase, a-amylase, β-glucanase, viscozyme®L, papain, compound protease, alkaline protease, neutral protease, chymotrypsin, catalase, trypsin, and pepsin). Extraction was performed at the optimal temperature and pH and at the medicinal powder: enzyme extract ratio of 1: 10. The enzyme-to-power ratio was 1: 100, and the shaking speed was set to 180 rpm. The optimal temperature and pH of enzymes were set in accordance with a previous study (Dai et al., 2019). The optimum temperature and pH of enzyme cellulase/viscozyme® L, compound protease/neutral protease, and chymotrypsin/trypsin are the same. Cellulase+viscozyme® L, compound protease + neutral protease, and chymotrypsin + trypsin were mixed separately and assisted in the extraction of active fractions. After 24 h shaking, the aqueous extracts of ginsengs were obtained. Proteins from the above extracts were removed by Sevag reagent. The active fraction was precipitation by 80% ethanol, and the precipitate was lyophilized and regarded as a crude aqueous extract (CAE).

Step-gradient ethanol precipitation was carried out for purification of the CAE in accordance with a previously described method (Fernando et al., 2020). Briefly, the CAE aqueous solution was adjusted to the ratio of 30% ethanol. The precipitate was harvested after 24 h of equilibrium time at 4 °C. Subsequently, the ratio of ethanol was increased to 60%, 80%, and 90% for precipitation.

Determination of DPPH, superoxide anion radical O^{2-}, and hydroxyl radical OH^-

The inhibitory capabilities of ethanol extracts and enzyme-assisted extracts of ginsengs on DPPH, O^{2-}, and OH^- were investigated following by the instructions of commercial kits.

Cell culture

H9c2(2-1) cardiomyocytes and C2C12 skeletal muscle-derived myoblasts were purchased from Wuhan Pnuosai Life Technology Co., LTD and incubated in 5% carbon dioxide at 37 °C in a constant temperature incubator. H9c2 and C2C12 cells were cultured in Dulbecco's Modified Eagle Medium (DMEM) (high-glucose DMEM medium + 10% fetal bovine serum +1% P/S). The differentiation medium (high-glucose DMEM medium + 2% horse serum +1% P/S) was used to differentiate C2C12 cells over a period of 5-7 days. Differentiation was confirmed by visualization of the formation of multinucleated myotubes.

Cytotoxicity and ROS production

The cytotoxicity of the extracts was determined via MTT assay, and intercellular ROS production was evaluated by DCFH-DA probe after PA explosion (Dai, Jiang, Lu, et al., 2020). Two cells in the PA group were added with 0.1, 0.2, 0.3, 0.4 and 0.5 mM PA to screen for the appropriate stimulating dose. The cells were seeded at a density of 1×10^6 cells/mL in a 96-well plate for 24 h and treated with the indicated concentrations of PA. The untreated cells were regarded as blank. After 24 h incubation, 50 μL of 2 mg/mL MTT solution was added to the cells. After another 3 h, the supernatant was discarded, and 200 μL of dimethyl sulfoxide was added to each well. The absorbance at 540 nm was determined by enzyme-linked immunosorbent assay to calculate the cell viability. Similarly, the cytotoxicity and ROS production of samples in PA-induced cells were determined by MTT and DCFH-DA assays, respectively.

Determinations of CK and LDH

To understand the protective effects of extracts on PA-induced cardiomyocytes and skeletal myoblasts, we evaluated the contents of CK and LDH in the two cell lines using commercial kits. Briefly, the cells were treated with PA and/or samples for 24 h. The contents of CK and LDH were determined by measuring the absorbance at 660 and 440 nm, respectively.

Glucose consumption and Oil Red O staining

Initially, the cardiomyocytes and differentiated skeletal myoblasts were seeded in serum-free and low-glucose

DMEM medium for 24 h starvation. The cells were treated with PA and/or samples for another 24 h period. The supernatant of each group was collected at 8, 16, 24, and 48 h for analysis. Glucose consumption in the supernatant was measured with a commercial kit.

Lipid droplets within cardiomyocytes and differentiated skeletal myoblasts were observed using Oil Red O staining. Briefly, the cells were washed with phosphate-buffered saline (PBS) and fixed with 4% formaldehyde for 20 min. The formaldehyde was substituted in PBS. Subsequently, the cells were washed with 60% isopropanol and kept for 5 min. Lipid droplets in cells were stained by Oil Red O for 30 min incubation, followed by two times of PBS washing. PBS was discarded, and cells were mounted with hematoxylin solution for nuclear staining. The stained cells were washed and imaged by a microscope (Olympus CKX53, Tokyo, Japan).

Determination of intracellular Ca^{2+} levels

In accordance with the instructions of commercial kits, the productions of Ca^{2+} in cardiomyocytes and differentiated skeletal myoblasts treated with PA and/or samples were evaluated with a fluo-8AM probe. The cell medium was discarded, and PBS solution containing 4 μM of fluo-8AM was added to the cells for 45 min incubation. Calcium production in each group was imaged by a fluorescent microscope (Olympus CKX53, Tokyo, Japan).

Hoechst 33342 and PI fluorescent staining assay

The cardiomyocytes and differentiated skeletal myoblasts were, respectively, treated with PA and/or samples in 6-well plates. PBS was used to wash the cells twice and substituted in the cell medium. Then, PBS was discarded, and Hoechst 33342 and PI were added to the cells for 20 min incubation in the dark. The cells were visualized by a fluorescent microscope (Olympus CKX53, Tokyo, Japan).

Evaluation of mitochondrial membrane potential (MMP)

Rhodamine 123 probe was used for MMP evaluation. Briefly, cardiomyocytes and differentiated skeletal myoblasts were treated with PA and/or samples for 24 h incubation. The medium was discarded and serum-free culture medium containing 0.1 μg/mL rhodamine 123 was used to mount cells for 45 min incubation at 37 °C. The cells were observed under a fluorescence microscope (Olympus CKX53, Tokyo, Japan).

Cell cycle assay

AnnexinV- FITC/PI probe was used to evaluate the cell cycle. Briefly, the cells were treated with PA and/or different concentrations of samples. After 24 h incubation, the cell medium was discarded, and the cells were washed thrice with pre-cooled PBS. The cell pellet was suspended in a binding buffer, and then continuously stained with PI and Annexin V-FITC for 15 min in the dark. The samples were analyzed within 1 h after staining. The cells were measured by a Cyto FLEX flow cytometer (Beckman Coulter Company, USA).

Western blotting analysis

After treatment with PA and/or samples, the cells were harvested and lysed with radioimmunoprecipitation assay lysis buffer. Cells containing 10 μg of protein were separated on sodium dodecyl sulfate-polyacrylamide gel electrophoresis gels. The gels loaded with proteins were transferred to polyvinylidene difluoride membranes, followed by blocking in skim milk. The membranes were incubated with primary antibody and kept at 4 °C overnight. Subsequently, the membrane was washed and mounted with the indicated secondary antibody based on the primary antibody for 1 h incubation. The membrane was imaged with a chemiluminescence solution in the dark and visualized by the Tanon 5200 automatic chemiluminescence imaging system (Shanghai Tianneng Technology Co., LTD, China). The intensities of proteins were calculated by ImageJ software.

Promoting effects on muscular endurance of zebrafish model

Origin and breeding of zebrafish

The wild-type AB line zebrafish and T*g* (kdrl:EGFP) zebrafish were purchased from Nanjing EzeRinka Biotechnology Co., LTD, and maintained at 28 °C with 14 h/10 h light/dark photoperiod. The feeding protocol of zebrafish was conducted following our previous report (Dai, Jiang, Nie, et al., 2020). All the animal experiments were in line with the Animal Care & Welfare Committee of Changchun University of Chinese Medicine (Approval No.: 2022647).

Protective effect of extracts in larvae

The T*g* (kdrl:EGFP) zebrafish (5 days post fertilization) were used to model the simulation of T2DM symptoms. The zebrafish were given 10% high-fat diet for 8 h and 3% glucose solution for 16 h in a day (every 24 h) (Wang et al., 2013). The feeding scheme was followed consecutively for 4 days, and the type 2 diabetic zebrafish model was established. The control group was given a normal commercial diet. In the sample-treated group, the zebrafish were administrated with a normal commercial diet, and the sample was dissolved in the medium. The medium in each well was replaced with a fresh one every 24 h.

The heart rate of zebrafish strongly influences the functional metabolism of their cardiomyocytes and skeletal myoblasts. Therefore, the indicated factors were recorded. In order to further verify whether the reduction of vascular lipid accumulation in type 2 diabetic patients with APMCG-1 is related to blood flow velocity, we treated 5dpf AB zebrafish with the modeling method described above. The Micro Zebra Lab application (view version 3.4.4, Lyon, France) is used to detect blood flow velocity in major blood vessels (Benslimane et al., 2020).

In accordance with the instructions of commercial kits, the contents of fasting blood glucose (FBG), TG, T-CHO, SOD, GSH-PX, CAT, MDA, TNF-a, IL-6, CK-MB, and cardiac troponin I cTnI were measured.

Protective effect of extracts on adult zebrafish

To further confirm the protective effect of extracts, we treated 1-month-old zebrafish (designed as "0 week") with a 1.75% glucose and 10% cholesterol diet for 4 weeks to establish a type 2 diabetic zebrafish model. The sample treatment group was given the indicated concentrations of extracts from 5th week to 8th week. The control group was fed a normal commercial diet. Zebrafish in each group were fed twice a day, and the medium was replaced with a fresh one group. After fasting for 12 h on the last day of the 8th week, the body weight of the zebrafish was measured. The muscular endurance of ginseng-treated zebrafish was evaluated following a previous method (Kim et al., 2019).

The zebrafish were euthanized by MS 222, and muscle tissue was collected for analysis. The levels of FBG, INS, TG, T-CHO, FFA, MG, SOD, GSH-PX, CAT, MDA, TNF-a and IL-6 were calculated following kit instructions.

In addition, the heart and muscle tissues of zebrafish in each group were collected and treated with 4% paraformaldehyde for 48 h. The hematoxylin-eosin (HE), TUNEL assay and DAPI staining, and immunohistochemistry (IHC) staining were performed by previous protocols (Li et al., 2018).

Characterization of active components

Chemical composition

Based on bioactivity screening, we selected the strongest promoting effect of the extract for chemical identification. Briefly, the qualitative assay results of carbohydrates, uronic acid, amino acids and peptides, ginsenosides, flavonoids, alkaloids and polyphenols in the samples were measured using previous standard procedures (Harborne, 1998).

Τηιν-λαψερ ςηροματογραπηψ ανδ β-ελιμινατιον

Thin-layer chromatography and β-elimination analysis were performed to identify glycopeptides, following a previous report (Kuritani et al., 2020). A 5 mL of 0.5 M hydrochloric acid containing 20 mg of extract was heated at 120 °C for 4 h. The solution was loaded on thin-layer chromatography plates as 0.8 cm streaks. The plates were run in n-butanol/acetone/acetic acid/5% ammonia/water (4.5:1.5:1:1:1.2), dried, and stained by

a chromogenic agent followed by re-drying and then heating in an oven at 105 °C for 5 min. The spots were visualized and photographed under sunlight.

Glycopeptide bond composition was identified by the β-elimination method (Zhu et al., 2020). The samples with or without alkali were dissolved in 0.4 M sodium hydroxide aqueous solution and held at 45 °C for 30 min incubation. The ultraviolet (UV) spectrum was measured. Alkali treatment was considered as the control.

Fourier transform infrared spectroscopy (FT-IR) analysis

The functional groups of the active components were analyzed by FT-IR. The samples (20 mg) and potassium bromide (100 mg) were mixed and pressed as tablets for analysis. The structure of samples was analyzed by OMNIC8.2 software.

Molecular weight determination

The molecular weight of the samples was determined by high-performance liquid chromatography (HPLC) and gel permeation chromatography (GPC). Dextran standards and 10 mg/mL of samples were dissolved in 0.7% sodium sulfate solution, and analyzed by a LC-2030C3D series HPLC (Shimadzu, Japan) system equipped with RID 20 and sepexsrtsec-100 column (7.8 × 300 mm, 5 μm) to determine the retention time. The column was maintained at 35 °C with 0.7% sodium sulfate solution as the mobile phase at a flow rate of 0.5 mL/min and an injection volume of 10 μL. The molecular weight of the sample was calculated by constructing a calibration curve in which the molecular weight log of glucan standards 180, 1000, 5000, 12000, 50000 and 64650 Da was plotted using the Agilent Chemical Station GPC Data Analysis software (Rev.A.02.01).

Derivatization of hydrolysates with 1-phenyl-3-methyl-5-pyrazolone (PMP)

The monosaccharide composition of the samples was determined by PMP derivatization following a previous method (B. Zhao et al., 2020). The mixture of 2 mL 2 M trifluoroacetic acid was mixed, and the samples were kept in an oven at 100 °C overnight for hydroxylation. After drying, 1mL of methanol was added to the residue, which was then dried using a nitrogen stream. The hydrolyzed sample was dissolved in 10 mL water for derivatization. The hydrolyzed sample was mixed with 5 mL 0.3 M sodium hydroxide. After 70 °C and 1 h incubation, the reaction mixture was neutralized with 5 mL of 0.3 M hydrochloric acid. The resulting solution was extracted thrice with chloroform and the aqueous layer was filtered and analyzed by HPLC (1260, Agilent, USA) equipped with Diamonsil C18 column (250 × 4.6mm, 5μm).

Amino acid determination

The amino acid composition of the samples was analyzed by using an A300 automatic amino acid analyzer (Membra Pure GmbH, Germany). Hydrochloric acid was employed to hydrolysis ginseng extract at 110 °C for 24 h. The hydrolyzed extract was filtered into a 25 mL volumetric flask. Then, 1 mL sample was absorbed and deacidified at 60 °C in a vacuum until a small amount of stain was left at the bottom. The tested buffer was added and mixed with the stain, and the resulting solution was filtered through a 0.45 μm filter for analysis.

Data processing

All experiments were repeated at least three times. Data were expressed as mean ± standard deviation and analyzed using GraphPad Prism 9. The mean values were analyzed by one-way analysis of variance. The mean values of the parameters were analyzed by student's t-test. $^{*}P < 0.05$, $^{**}P < 0.01$, and $^{***}P < 0.001$ indicated a significant difference.

Results

Radical scavenging activities of active fractions

The ethanol extracts of RG, CG, and MCG were patriated by different polarity solutions involving hexane, chloroform, ethyl acetate,*n* -butanol and residual water-layer extracts. Fifteen fractions were obtained. A total of 48 CAEs were collected from sixteen kinds of enzyme-assisted ginseng residues.

All fifteen ethanol extracts showed low scavenging activities. Among the 48 CAEs, the scavenging capability of OH^- in the three ginsengs showed stronger activities than those of DPPH and O^{2-}. Among the sixteen kinds of enzymes, alkaline protease-assisted extract of MCG (APMCG) demonstrated the highest inhibitory effect on OH^- in a dose-dependent manner (Fig. 1A, 1B, 1C). Four active factions were harvested from the step-gradient ethanol precipitation at ratios of 30%, 60%, 80%, and 90%, and they named APMCG-1, APMCG-2, APMCG-3, and APMCG-4, respectively. As shown in Fig.1D, APMCG-1 demonstrated the most marked inhibitory effect on OH^- (84.16%).

Cytotoxicity and protective effects of APMCG *in vitro*

Based on the strong scavenging activity of the four fractions, APMCG, APMCG-1, APMCG-2, APMCG-3, and APMCG-4 were selected for further*in vitro* assay. Initially, different concentrations of PA were screened, and the PA concentration of 0.2 mM was selected because its cell viability was 60% (Fig. 2A). The treatment concentration of samples was set from 6.25 μg/mL to 100 μg/mL. All concentrations of the samples showed low toxic except concentration of 100 μg/mL (Fig. 2B). Fractions ranging from 6.25 μg/mL to 50 μg/mL significantly increased cell viabilities in PA-induced H9c2 cells, implicating a strong cardioprotective effect on cardiomyocytes (Fig. 2C). Especially, the concentrations of APMCG-1 markedly down-regulated intracellular ROS production and LDH content in PA-induced H9c2 cells dose-dependently, revealing strong protection against oxidative caused injury (Fig. 2D, 2E). Oil Red O staining revealed that PA resulted in shrinking, rounding, and shedding of H9c2 cells, as observed via an inverted microscope. After APMCG-1 treatment, the intracellular lipid accumulation of PA-induced H9c2 cells decreased (Fig. 2F). Compared with that in the untreated group, no significant difference was observed in the AKT level in each group of H9c2 cells, whereas p-AKT significantly increased in PA-induced H9c2 cells after APMCG-1 treatment (Fig. 2G). Thus, APMCG-1exhibits a cardioprotective effect by regulation of AKT/p-AKT signaling protein. We employed PI3K/AKT inhibitors to determine whether the inhibitory impact of APMCG-1 on PA-induced apoptosis in H9c2 cells was due to the PI3K/AKT signaling pathway (Wei et al., 2012). The cells were pretreated with 10 μM LY294002 for 1 h, followed by 1 h of treatment with 50 μg/mL APMCG-1 and 24 h of treatment with PA. The outcomes demonstrate that the reduction in p-AKT level caused by 50 μg/mL APMCG-1. According to the aforementioned findings, APMCG-1 can partially prevent PA from inducing the death of H9c2 cells through activating the PI3K/AKT signaling pathway (Fig. 2H).

Similarly, a 0.2 mM PA was selected for the simulating C2C12 cell damage (Fig. 2I). As shown in Fig. 2J and Fig. 2K, the indicated concentrations of active fraction showed low cytotoxicity, and APMCG-1 significantly increased cell viability in damaged PA-induced C2C12 cells. Meanwhile, APMCG-1 reduced the CK content compared with that in the PA-treated group in a dose-dependent manner, implicating the alleviation of insulin resistance and microcirculation disorders in the skeletal muscle (Fig. 2L). In addition, APMCG-1 significantly increased cellular glucose consumption at 8, 16, 24, and 48 h in time- and dose-dependent manners compared with the model group, suggesting that it attenuated high glucose-induced damage (Fig. 2M). Fig. 2N shows that different concentrations of APMCG-1 decreased intracellular lipid accumulation in PA-induced C2C12 cells. Western blotting showed that the expressions of IRS1, PI3K, AKT and GLUT4 in PA-induced C2C12 cells were up-regulated by APMCG-1 treatment (Fig. 2O). These results revealed that APMCG-1 activates the PI3K/AKT signaling pathway to promote the survival and function of cardiomyocytes and skeletal myoblasts.

APMCG-1 attenuates ER and mitochondrial dysfunction in cardiomyocytes and skeletal muscles

ER is the main location for the storage of calcium ions in cardiomyocytes, and the apoptosis pathway mediated by ER is bound to be related to calcium ions (Groenendyk et al., 2021). As shown in Fig. 3A, the four indicated concentrations of APMCG-1 reduced PA-induced intracellular Ca^{2+} levels in H9c2 cells,

which reflected the reduction of Ca^{2+} levels in the cytoplasm. The key signals of ER stress pathway, which involvs to GRP78, p-PERK, p-eIF2a, ATF4 and CHOP in PA-induced H9c2 cells significantly increased. However, when the cells were pretreated with APMCG-1, the levels of these signal proteins all decreased (Fig. 3B). Hoechst 33342 and PI staining showed abnormal morphology and nuclear condensation in PA-induced H9c2 cells. With the increased concentration of APMCG-1, the fluorescence intensity gradually decreased, implying that APMCG-1 can repair PA-induced nuclear condensation (Fig. 3C, 3D). Excessive ER stress causes the release of Ca^{2+} from the ER to specific structures of mitochondria, which initiates the caspase cascade and ultimately leads to apoptosis. Thus, a rhodamine 123 fluorescent probe was used to evaluate mitochondrial dysfunction. Visualization of untreated H9c2 cells by a fluorescence microscope showed a bright green fluorescence around the nucleus. The bright green fluorescence in PA-induced H9c2 cells significantly decreased, indicating the loss of MMP. However, the fluorescence intensity increased after the pretreatment with APMCG-1 (Fig. 3E). In flow cytometry analysis of PA-induced H9c2 cells, APMCG-1 significantly reduced the proportion of early apoptotic cells against PA-induced mitochondrial apoptosis (Fig. 3F). The caspase family plays a key role in cell apoptosis and regulates cell apoptosis together with a variety of protein factors. The expressions of Bax, Bcl2 and Cleaved-Caspase3 of H9c2 cells were significantly decreased in APMCG-1-treated PA-induced H9c2 cells (Fig. 3G). These results illustrate that the Bax family signaling pathway is required for APMCG-1 to enhance ER and mitochondrial function in the cardiomyocytes.

We collected each group of cells and treated them with 2.5% glutaraldehyde fixed solution at room temperature in order to examine the ultra-structure of the cells using a transmission electron microscope (HT7700, HITACHI, Japan) in order to assess the ER stress and mitochondrial apoptosis in H9c2 cell (Jung & Mun, 2019). The findings demonstrated that the control group had healthy cardiomyocytes with intact mitochondria and ER. The model group's myocardial cells displayed evident damage, swollen and vacuolated mitochondria, and expanded ER. The amount of healthy mitochondria and ER in H9c2 cells gradually increased as APMCG-1 concentration rose (Fig. 3H).

Meanwhile, APMCG-1 exhibited a strong protective property against in mitochondrial dysfunction in skeletal muscles. We characterized the morphological changes in PA-induced C2C12 cells (Fig. 3I and 3J). The morphology of cell death observed by fluorescence microscopy implied the APMCG-1 protection against PA-induced C2C12 cell damage. Further, the results showed that APMCG-1 up-regulated MMP (Fig. 3K) and down-regulated the number of apoptotic cells (Fig. 3L). In addition, APMCG-1 reduced the expression levels of Cleaved-Caspase3, Cleaved-Caspase9, and Bax/Bcl2 in PA-induced C2C12 cells, suggesting the action of APMCG-1 against PA-induced endogenous apoptosis (Fig. 3M). On the basis of the above information, we concluded that APMCG-1 enhances mitochondrial biosynthesis in skeletal myoblasts.

APMCG-1 improves cardiomyocytes in larvae

To validate whether APMCG-1 normalizes cardiomyocytes and skeletal myoblasts capacities, we analyzed the functional and energy metabolism in of type 2 diabetic zebrafish model. The heart rate of zebrafish refers to the heart beats per minute, and the change in heart rate is an important index for the evaluation of cardiac function. Compared with that of the untreated group, the heart rate of zebrafish in the model group decreased, and the mortality increased. Compared with the model group, different concentrations of APMCG-1 increased the heart rate and decreased mortality (Fig. 4A, 4B). After five days of continuous high-cholesterol feeding, accumulation of lipid deposition was observed at the bifurcation of blood vessels, which indicated that high blood lipid levels can promote and cause the occurrence of atherosclerosis and lead to the localization of atherosclerosis (Fig. 4C). The blood flow rate of larvae in the model group was significantly decreased, and the decreased blood flow rate was significantly recovered after 50 μg/mL APMCG-1 treatment (Fig. 4D). Therefore, 50 μg/mL APMCG-1 was selected for follow-up experiments.

Insulin resistance is an independent risk factor for diabetes. Compared with the model group, the increased concentrations of APMCG-1 decreased the levels of FBG, T-CHO, and TG dose-dependently in the treated group. This finding illustrates that APMCG-1 regulated blood glucose and lipid levels in type 2 diabetic zebrafish. CK-MB is a subtype of CK that is found only in the heart and cTnI is a specific marker of myocardial necrosis. Thus, CK-MB and cTnI are associated with myocardial injury. We observed that APMCG-1

markedly decreased the levels of CK-MB and cTnI compared with those in the model zebrafish, which revealed that APMCG-1 can reduce cardiac injury (Fig. 4E). Compared with the model group, APMCG-1 significantly increased the levels of SOD, GSH-PX and CAT, and decreased the level of MDA, TNF-a and IL-6 in the treatment group (Fig. 4F). Collectively, the data suggested that APMCG-1 predominately promotes glucose uptake and metabolism in cardiomyocytes and skeletal myoblasts.

APMCG-1 normalizes muscle capacity in T2DM zebrafish

The main causes of insulin resistance include abnormal fat metabolism, abnormal fat distribution and excessive accumulation. The body weight of APMCG-1-treated zebrafish was significantly decreased compared with that of the model group (Fig. 5A). According to the determination of swimming endurance, it was found that APMCG-1 enhanced swimming endurance compared with the model group (Fig. 5B). The FBG, INS, T-CHO, TG, FFA and MG of zebrafish in the APMCG-1-treated group significantly decreased, and MG was significantly increased, indicating that APMCG-1 improved the symptoms of insulin resistance in type 2 diabetic zebrafish (Fig. 5C). Meanwhile, the levels of SOD, GSH-PX and CAT levels increased, and that of MDA, TNF-a and IL-6 decreased in the APMCG-1 group, demonstrating that APMCG-1 improved the oxidant-induced muscle injury (Fig. 5D). In the control group, the heart and skeletal muscle structure were complete and the muscle fibers were arranged neatly. In the model group, muscle fibers were disordered and broken. Compared with the model group, APMCG-1 alleviated the pathological damage of heart and skeletal muscle and muscle fiber breakage in type 2 diabetic zebrafish (Fig. 5E, 5F). The results of IHC showed that APMCG-1 could also increase the expression of AKT in skeletal muscle tissue (Fig. 5G). The cells of zebrafish in the control group showed normal size, high density and less apoptosis. In the model group, the number of apoptotic cells were increased and showed sparse. Whereas, the apoptosis of cells in zebrafish treated with APMCG-1 were gradually decreased (Fig. 5H, 5I). Altogether, *in vivo* results confirmed that APMCG-1 treatment significantly protects cardiomyocytes and skeletal myoblasts in type 2 diabetes.

Characterization of APMCG-1

The chemical composition of APMCG-1 was analyzed and the following contains were observed: 0.85% alkaloids, 25.98% amino acids and peptides, 39.8% carbohydrates, 0.95% flavonoids, 0.3% polyphenols, 1.47% saponins, 15% uronic acids, and 15.63% unknown (Fig. 6A). To identify the presence or absence of glycopeptides in APMCG-1, we used β-elimination reaction. The results showed that the absorption value of the UV spectrum of APMCG-1 significantly increased at 240 nm after alkali treatment, and contained O-linked glycopeptide bonds (Fig. 6B). The results of thin-layer chromatography analysis showed that APMCG-1 also contained sugars and peptides. As revealed by the FT-IR spectrum, the strong and broad absorption peak at around 3400 cm^{-1} indicated the stretching vibration peak of -OH or -NH on the polysaccharide. The moderate-intensity absorption peak at 2920 cm^{-1} marked the stretching vibration peak of -CH_2 and -CH. The absorption peaks at 1600 cm^{-1} implied the asymmetric stretching vibration peaks caused by C=O. The above absorption peaks were characteristics of polysaccharides. The absorption peak at 1400 cm^{-1} was caused by the deprotonated carboxyl group, indicating the presence of a uronic acid structure. The absorption peak at 760 cm^{-1}represented the absorption peak of pyran-ring symmetric ring stretching vibration, revealing the presence of pyran polysaccharide (Fig. 6C). The retention times of mannose, rhamnose, glucuronic acid, galacturonic acid, glucose, xylose, galactose, and fucose were observed at 13.120, 16.678, 21.075, 25.187, 30.560, 34.898, 35.640, 38.224 and 42.174 min, respectively. The ratio of monosaccharide of APMCG-1 was mannose, rhamnose, galacturonic acid, glucose, xylose, galactose and arabinose 1:2.57:15:24.54:3.4:28.54:12.38 (Fig. 6D). Amino acid involving cysteic acid, methionine alum, aspartic acid, threonine, serine), glutamate, glycine, alanine, cysteine, valine), methionine, isoleucine, leucine, tyrosine, phenylalanine, histidine, lysine, arginine and proline were used as the standard substance, the amino acid composition of APMCG-1 was composed of aspartic acid (2.797%), methionine (3.271%), phenylalanine (6.503%), histidine (4.748%), arginine (2.513%), proline (1.433%), and NH4 (9.086%) (Fig. 6E). These findings denote that APMCG-1 is an active glycopeptide isolated from MCG.

Discussions

Ginseng's quality mostly depends on elements including its wild kind, cultivation, age, and technique of processing. CG and MCG are grown in gardens for 4-6 years and mountainous forests for over 20 years, respectively. However, it is still unclear how MCG reduces the dysfunction of the skeletal myoblast and cardiomyocyte. The activation of the AKT, PI3K, and mTOR signaling pathway is an approach for the treatment of skeletal muscle atrophy in people with diabetes, according to clinical and experimental evidence. Therefore, it is important to look into how T2DM circumstances affect the functional alterations that occur in cardiomyocytes and skeletal myoblasts.

This work, revealed the unreported property of APMCG-1 as an AKT activator in the protection against oxidant stress not only in cardiomyocytes but also in skeletal myoblasts under T2DM conditions. Importantly, on the basis of these findings, we proposed a model of biological adaptation in which cardiomyocytes and skeletal myoblasts pretreated with APMCG-1 can induce the enhancement of glucose uptake, ER metabolism and mitochondrial biosynthesis and consequently protect oxidant stimulated injury through regulation of the PI3K/AKT signaling pathway.

TCM industries produce large amounts of herbal extraction residues, which amount to approximately millions of tons of solid waste annually (Meng et al., 2017). The residues without well-designed management indirectly or directly contaminate groundwater and soil. These "waste residues" contain certain amounts of bio-resources, and have great potential as feedstock to generate various valuable and useful products. Researchers believe that the quality and price of MCG are considerably higher than those of CG (Lu & Li, 2021). In recent years, report focused that industrial herbal waste should advance management, but a strategy for recycling MCG is unclear (Huang et al., 2021). We designed and performed a systematic extraction protocol for three kinds of ginsengs, and explored their ethanol- and water-soluble compounds. The ethanol-extracted MCG residue was extracted again by water to obtain water-soluble compounds. APMCG-1 was first obtained from the ethanol-extracted MCG residue. Meanwhile, APMCG-1 was found to contain polysaccharide and proteins, which are connected by O-linked glycopeptide bonds. Seven indicated monosaccharides and seven amino acids were found in APMCG-1. Hence, the novel extraction method for APMCG-1 was performed and the potential biological properties of APMCG-1 are highly expected.

Importantly, we have confirmed the activation of AKT by APMCG-1 in cardiac and skeletal muscle cells and zebrafish models under type 2 diabetic conditions. AKT has been proposed to inhibit ER stress and apoptosis by activating PI3K, which is important for the regulation of ER biogenesis, particularly in rat cardiomyocytes (Liang et al., 2008). Previous reports revealed that PA reduced insulin-induced phosphorylation of AKT, and stimulated ER stress and mitochondrial dysfunction in myoblasts (Peng et al., 2011; Yen et al., 2012). Moreover, insulin regulates heart metabolism through the regulation of insulin-induced glucose uptake, leading to mitochondrial fusion via the AKT-mTOR-nuclear factor-ϰB-Opa-1 pathway (Parra et al., 2014). Consistent with these results, our study demonstrated that APMCG-1 enhanced glucose uptake through the downregulation of CK-MB and cTnI in cardiomyocytes and neurons. Moreover, the Western blotting analysis demonstrated that APMCG-1 evidently increased expressions of IRS1, PI3K, AKT and GLUT4, which suggest that APMCG-1 caused the increases in cardiac and skeletal muscle glucose uptake.

Overexpression or activation of the PI3K/AKT/mTOR signaling pathway suppresses ER stress, apoptosis, and autophagy in diabetic cardiomyopathy (G. Zhao et al., 2020). In our study, consistent with the data on cell viability and ROS, APMCG-1 decreased PA-induced intracellular Ca^{2+} levels in PA-induced H9c2 cells, attenuating ER-dependent cell apoptosis. Moreover, calcium ion regulates non-gene transcription and is involved in cell growth, differentiation and proliferation. Stored Ca^{2+} plays an essential role in apoptosis-associated Bcl2 activation by regulating the two-way cross-talk between the mitochondria and ER (Wu et al., 2015). Previous disconcerting reports regarding an approach to increasing skeletal myoblast viability after transplantation in the ischemic heart have reached minimal success, with approximately 20% of the live skeletal myoblasts left within 72h (Niagara et al., 2007). Intriguingly, the evidence showed that APMCG-1 both protects skeletal myoblasts and cardiomyocytes from oxidant-induced damage, which suggests that APMCG-1 can serve as a complementary agent in the strategies. Collectively, we observed that APMCG-1 pretreatment restored ER and mitochondrial function under normal circumstances to resist

diabetic injury with the reduction of ROS production and mitochondrial apoptosis based on the*in vitro* and *in vivo* observations.

Conclusions

In this study, APMCG-1 was first isolated from ethanol-extracted MCG residue. The functional promotion of APMCG-1 in cardiomyocytes and skeletal myoblasts was systemically explored. Through the PI3K/AKT signaling pathway, APMCG-1 decreases palmitic acid-induced apoptosis in H9c2 and C2C12 cells. In type 2 diabetic zebrafish, APMCG-1 can reduce the levels of cardiac and muscle apoptosis, oxidative stress, inflammation, and glucose lipid metabolism problem. Further, chemical and structural analyses confirmed the presence of polysaccharides and peptides in APMCG-1, and we demonstrated that APMCG-1 is a glycopeptide. Therefore, the present findings proved that APMCG-1 may have attractive significance for the prevention and treatment of muscle-related diseases.

References

Abel, E. D. (2018). MITOCHONDRIAL DYNAMICS AND METABOLIC REGULATION IN CARDIAC AND SKELETAL MUSCLE. *Trans Am Clin Climatol Assoc* ,*129* , 266-278.

Benslimane, F. M., Zakaria, Z. Z., Shurbaji, S., Abdelrasool, M. K. A., Al-Badr, M., Al Absi, E. S. K., & Yalcin, H. C. (2020). Cardiac function and blood flow hemodynamics assessment of zebrafish (Danio rerio) using high-speed video microscopy. *Micron* , *136* , 102876.*https://doi.org/10.1016/j.micron.2020.102876*

Cui, Q. N., Stein, L. M., Fortin, S. M., & Hayes, M. R. (2022). The role of glia in the physiology and pharmacology of glucagon-like peptide-1: implications for obesity, diabetes, neurodegeneration and glaucoma. *Br J Pharmacol* , *179* (4), 715-726.*https://doi.org/10.1111/bph.15683*

Dai, Y. L., Jiang, Y. F., Lee, H. G., Jeon, Y. J., & Kang, M. C. (2019). Characterization and screening of anti-tumor activity of fucoidan from acid-processed hijiki (Hizikia fusiforme). *Int J Biol Macromol* , *139* , 170-180.*https://doi.org/10.1016/j.ijbiomac.2019.07.119*

Dai, Y. L., Jiang, Y. F., Lu, Y. A., Kang, M. C., & Jeon, Y. J. (2020). Fucoidan from acid-processed Hizikia fusiforme attenuates oxidative damage and regulate apoptosis. *Int J Biol Macromol* , *160* , 390-397.*https://doi.org/10.1016/j.ijbiomac.2020.05.143*

Dai, Y. L., Jiang, Y. F., Nie, Y. H., Lu, Y. A., & Jeon, Y. J. (2020). Hepato-protective effect of fucoidan extracted from acid-processed Sargassum fusiformis in ethanol-treated Chang liver cells and in a zebrafish model. *Journal of Applied Phycology* , *32* (6).

Fernando, I. P. S., Dias, M., Madusanka, D. M. D., Han, E. J., Kim, M. J., Jeon, Y. J., & Ahn, G. (2020). Step gradient alcohol precipitation for the purification of low molecular weight fucoidan from Sargassum siliquastrum and its UVB protective effects. *Int J Biol Macromol* ,*163* , 26-35.*https://doi.org/10.1016/j.ijbiomac.2020.06.232*

Frontera, W. R., & Ochala, J. (2015). Skeletal muscle: a brief review of structure and function. *Calcif Tissue Int* , *96* (3), 183-195.*https://doi.org/10.1007/s00223-014-9915-y*

Groenendyk, J., Agellon, L. B., & Michalak, M. (2021). Calcium signaling and endoplasmic reticulum stress. *Int Rev Cell Mol Biol* , *363* , 1-20.*https://doi.org/10.1016/bs.ircmb.2021.03.003*

Harborne, J. B. (1998). Tony Swain and phytochemical methods.

Huang, C., Li, Z. X., Wu, Y., Huang, Z. Y., Hu, Y., & Gao, J. (2021). Treatment and bioresources utilization of traditional Chinese medicinal herb residues: Recent technological advances and industrial prospect.*J Environ Manage* , *299* , 113607.*https://doi.org/10.1016/j.jenvman.2021.113607*

Jiao, W., Mi, S., Sang, Y., Jin, Q., Chitrakar, B., Wang, X., & Wang, S. (2022). Integrated network pharmacology and cellular assay for the investigation of an anti-obesity effect of 6-shogaol. *Food Chem* ,*374* , 131755.*https://doi.org/10.1016/j.foodchem.2021.131755*

Jung, M., & Mun, J. Y. (2019). Mitochondria and Endoplasmic Reticulum Imaging by Correlative Light and Volume Electron Microscopy. *J Vis Exp* (149).*https://doi.org/10.3791/59750*

Kim, S.-Y., Kim, H.-S., Cho, M., & Jeon, Y.-J. (2019). Enzymatic Hydrolysates of Hippocampus abdominalis Regulates the Skeletal Muscle Growth in C2C12 Cells and Zebrafish Model. *Journal of Aquatic Food Product Technology* , *28* , 1-11.*https://doi.org/10.1080/10498850.2019.1575940*

Kuritani, Y., Sato, K., Dohra, H., Umemura, S., Kitaoka, M., Fushinobu, S., & Yoshida, N. (2020). Conversion of levoglucosan into glucose by the coordination of four enzymes through oxidation, elimination, hydration, and reduction. *Sci Rep* , *10* (1), 20066.*https://doi.org/10.1038/s41598-020-77133-8*

Lee, H. G., Kim, H. S., Oh, J. Y., Lee, D. S., Yang, H. W., Kang, M. C., Kim, E. A., Kang, N., Kim, J., Heo, S. J., & Jeon, Y. J. (2021). Potential Antioxidant Properties of Enzymatic Hydrolysates from Stichopus japonicus against Hydrogen Peroxide-Induced Oxidative Stress.*Antioxidants (Basel)* , *10* (1).*https://doi.org/10.3390/antiox10010110*

Li, X., Zhong, L., Wang, Z., Chen, H., Liao, D., Zhang, R., Zhang, H., & Kang, T. (2018). Phosphorylation of IRS4 by CK1γ2 promotes its degradation by CHIP through the ubiquitin/lysosome pathway. *Theranostics* , *8* (13), 3643-3653.*https://doi.org/10.7150/thno.26021*

Liang, C. S., Mao, W., & Liu, J. (2008). Pro-apoptotic effects of anti-beta1-adrenergic receptor antibodies in cultured rat cardiomyocytes: actions on endoplasmic reticulum and the prosurvival PI3K-Akt pathway. *Autoimmunity* , *41* (6), 434-441.*https://doi.org/10.1080/08916930802031710*

Lu, Q., & Li, C. (2021). Comprehensive utilization of Chinese medicine residues for industry and environment protection: Turning waste into treasure. *Journal of Cleaner Production* , *279* , 123856.*https://doi.org/https://doi.org/10.1016/j.jclepro.2020.123856*

Meng, F., Yang, S., Wang, X., Chen, T., Wang, X., Tang, X., Zhang, R., & Shen, L. (2017). Reclamation of Chinese herb residues using probiotics and evaluation of their beneficial effect on pathogen infection. *J Infect Public Health* , *10* (6), 749-754.*https://doi.org/10.1016/j.jiph.2016.11.013*

Niagara, M. I., Haider, H., Jiang, S., & Ashraf, M. (2007). Pharmacologically preconditioned skeletal myoblasts are resistant to oxidative stress and promote angiomyogenesis via release of paracrine factors in the infarcted heart. *Circ Res* , *100* (4), 545-555.*https://doi.org/10.1161/01.RES.0000258460.41160.ef*

Ohsaki, Y., Sołtysik, K., & Fujimoto, T. (2017). The Lipid Droplet and the Endoplasmic Reticulum. *Adv Exp Med Biol* , *997* , 111-120.*https://doi.org/10.1007/978-981-10-4567-7_8*

Parra, V., Verdejo, H. E., Iglewski, M., Del Campo, A., Troncoso, R., Jones, D., Zhu, Y., Kuzmicic, J., Pennanen, C., Lopez-Crisosto, C., Jaña, F., Ferreira, J., Noguera, E., Chiong, M., Bernlohr, D. A., Klip, A., Hill, J. A., Rothermel, B. A., Abel, E. D., Zorzano, A., & Lavandero, S. (2014). Insulin stimulates mitochondrial fusion and function in cardiomyocytes via the Akt-mTOR-NFκB-Opa-1 signaling pathway. *Diabetes* , *63* (1), 75-88.*https://doi.org/10.2337/db13-0340*

Peng, G., Li, L., Liu, Y., Pu, J., Zhang, S., Yu, J., Zhao, J., & Liu, P. (2011). Oleate blocks palmitate-induced abnormal lipid distribution, endoplasmic reticulum expansion and stress, and insulin resistance in skeletal muscle. *Endocrinology* , *152* (6), 2206-2218.*https://doi.org/10.1210/en.2010-1369*

Phielix, E., & Mensink, M. (2008). Type 2 diabetes mellitus and skeletal muscle metabolic function. *Physiol Behav* , *94* (2), 252-258.*https://doi.org/10.1016/j.physbeh.2008.01.020*

Sinacore, D. R., & Gulve, E. A. (1993). The role of skeletal muscle in glucose transport, glucose homeostasis, and insulin resistance: implications for physical therapy. *Phys Ther* , *73* (12), 878-891.*https://doi.org/10.1093/ptj/73.12.878*

Sun, J., Zhong, X., Sun, D., Cao, X., Yao, F., Shi, L., & Liu, Y. (2022). Structural characterization of polysaccharides recovered from extraction residue of ginseng root saponins and its fruit nutrition preservation

performance. *Front Nutr* , *9* , 934927.*https://doi.org/10.3389/fnut.2022.934927*

Tao, W., Jin, J., Zheng, Y., & Li, S. (2021). Current Advances of Resource Utilization of Herbal Extraction Residues in China. *Waste and Biomass Valorization* (3).

Wang, Z., Mao, Y., Cui, T., Tang, D., & Wang, X. L. (2013). Impact of a combined high cholesterol diet and high glucose environment on vasculature. *PLoS One* , *8* (12), e81485.*https://doi.org/10.1371/journal.pone.0081485*

Wei, C. D., Li, Y., Zheng, H. Y., Sun, K. S., Tong, Y. Q., Dai, W., Wu, W., & Bao, A. Y. (2012). Globular adiponectin protects H9c2 cells from palmitate-induced apoptosis via Akt and ERK1/2 signaling pathways.*Lipids Health Dis* , *11* , 135.*https://doi.org/10.1186/1476-511x-11-135*

Wu, H., Ye, M., Yang, J., Ding, J., Yang, J., Dong, W., & Wang, X. (2015). Nicorandil Protects the Heart from Ischemia/Reperfusion Injury by Attenuating Endoplasmic Reticulum Response-induced Apoptosis Through PI3K/Akt Signaling Pathway. *Cell Physiol Biochem* , *35* (6), 2320-2332.*https://doi.org/10.1159/000374035*

Xu, X. F., Cheng, X. L., Lin, Q. H., Li, S. S., Jia, Z., Han, T., Lin, R. C., Wang, D., Wei, F., & Li, X. R. (2016). Identification of mountain-cultivated ginseng and cultivated ginseng using UPLC/oa-TOF MSE with a multivariate statistical sample-profiling strategy. *J Ginseng Res* , *40* (4), 344-350.*https://doi.org/10.1016/j.jgr.2015.11.001*

Yen, Y. P., Tsai, K. S., Chen, Y. W., Huang, C. F., Yang, R. S., & Liu, S. H. (2012). Arsenic induces apoptosis in myoblasts through a reactive oxygen species-induced endoplasmic reticulum stress and mitochondrial dysfunction pathway. *Arch Toxicol* , *86* (6), 923-933.*https://doi.org/10.1007/s00204-012-0864-9*

Yi, Y. S. (2022). Potential benefits of ginseng against COVID-19 by targeting inflammasomes. *J Ginseng Res* , *46* (6), 722-730.*https://doi.org/10.1016/j.jgr.2022.03.008*

Zhang, L., Keung, W., Samokhvalov, V., Wang, W., & Lopaschuk, G. D. (2010). Role of fatty acid uptake and fatty acid beta-oxidation in mediating insulin resistance in heart and skeletal muscle. *Biochim Biophys Acta* , *1801* (1), 1-22.*https://doi.org/10.1016/j.bbalip.2009.09.014*

Zhao, B., Wang, X., Liu, H., Lv, C., & Lu, J. (2020). Structural characterization and antioxidant activity of oligosaccharides from Panax ginseng C. A. Meyer. *Int J Biol Macromol* , *150* , 737-745.*https://doi.org/10.1016/j.ijbiomac.2020.02.016*

Zhao, G., Zhang, X., Wang, H., & Chen, Z. (2020). Beta carotene protects H9c2 cardiomyocytes from advanced glycation end product-induced endoplasmic reticulum stress, apoptosis, and autophagy via the PI3K/Akt/mTOR signaling pathway. *Ann Transl Med* , *8* (10), 647.*https://doi.org/10.21037/atm-20-3768*

Zhu, L., Li, J., Wang, Y., Sun, X., Li, B., Poungchawanwong, S., & Hou, H. (2020). Structural feature and self-assembly properties of type II collagens from the cartilages of skate and sturgeon. *Food Chemistry* , *331* , 127340.*https://doi.org/https://doi.org/10.1016/j.foodchem.2020.127340*

Hosted file

`Figure Legends.doc` available at https://authorea.com/users/582398/articles/622472-glycopeptide-from-mountain-cultivated-ginseng-attenuates-oxidant-induced-cardiomyocyte-and-skeletal-myoblast-injury